

Supplementary Information: Free energy from stationary implementation of the DFT+DMFT functional

Kristjan Haule and Turan Birol

Department of Physics and Astronomy, Rutgers University, Piscataway, USA

(Dated: today)

PACS numbers:

TECHNICAL DESCRIPTION OF COMPUTATIONAL DETAILS

We used the implementation of LDA+DMFT of Ref.1, which is based on Wien2K package [2]. The exchange-correlation functional E_{xc} of LDA was utilized, in combination with nominal double-counting (DC) [1, 3], which was shown to be closest to the exact form of DC [4]. We checked (on the example of Cerium) that the exact-DC gives very similar free energy, as expected for a stationary functional. The convergence of LDA+DMFT results is much faster using nominal DC, hence most of results in this publication are obtained by this simplification.

The impurity model is solved using the hybridization expansion version of the numerically exact continuous time QMC method [5, 6]. Of the order of 300 LDA and 30 DMFT iterations were required for precision of 1 meV per formula unit, and between $10^9 - 10^{10}$ Monte Carlo moves were accepted per impurity iteration for precise enough impurity solution. The resources of Titan supercomputer were used.

To construct the projector, the atomic-like local orbitals are used $\langle \mathbf{r} | \phi_{lm} \rangle = \frac{u_l(r)}{r} Y_{lm}(\hat{\mathbf{r}})$. The radial part of the local orbital $u_l(r)$ is the solution of the scalar relativistic Dirac equation inside the muffin-tin sphere, linearized at the Fermi level. The muffin-tin spheres are set to touch at the lowest volume. We tested a few other forms of the projectors defined in Ref. 1. The stationary $F(V)$ is quite insensitive to the precise choice of projector, however, $E(V)$ changes much more.

For SrVO₃ calculations, we treated dynamically all five

$3d$ orbitals of Vanadium. The muffin-tin radius of Vanadium was set to $R_{mt} = 1.83 a_B$, and $U = 10$ eV was used, which was previously shown to give good spectra [3, 4] for this localized orbital (see spectra below). The Yukawa form of screening interaction than gives $J \approx 1$ eV (see note below). Brillouin zone integrations were done over $15 \times 15 \times 15$ k-point in the whole zone in the self-consistent calculations, and for calculation of the impurity entropy, the hybridization is computed on more precise $36 \times 36 \times 36$ k-points mesh. We mention in passing that impurity entropy is very sensitive to the precise frequency dependence of the hybridization, and requires very dense momentum mesh.

For FeO, all five $3d$ orbitals are treated by DMFT and the muffin-tin radius of iron is set to $R_{mt} = 2.11 a_B$, and the Coulomb repulsion to previously determined $U = 8$ eV [7], which requires $J \approx 1$ eV in Yukawa form. In Ce metal, all seven $4f$ orbitals are treated by DMFT and the muffin-tin sphere is $R_{mt} = 2.5 a_B$, the k-point mesh is $21 \times 21 \times 21$, and the Coulomb $U = 6$ eV [8–10], leads to $J = 0.72$ eV in Yukawa form. The spin-orbit coupling is included in Cerium, but neglected in SrVO₃ and FeO.

DETAILS ON EVALUATION OF LDA+DMFT FUNCTIONAL

Here we explain how we evaluate the total energy Eq.1 and the free energy Eq.4 of the main text.

For total energy Eq.1, we group the terms in the following way

$$E = \text{Tr}((-\nabla^2 + V_{ext} + V_H + V_{xc})G) - \text{Tr}((V_H + V_{xc})\rho) + E^H[\rho] + E^{xc}[\rho] + E_{nuc-nuc} + \frac{1}{2}\text{Tr}(\Sigma G) - \Phi^{DC}[\rho_{loc}] \quad (1)$$

We then split the energy into three terms $E = E_1 + E_2 + E_3$, where the first two parts E_1, E_2 are computed using the Green's function of the solid, and the third E_3 using the impurity Green's function.

The first five terms in Eq. 1 look similar to the standard DFT energy functional, except that the Green's function G here is the self-consistent LDA+DMFT Green's

function. We first solve the eigenvalue problem for Kohn-Sham states $(-\nabla^2 + V_{ext} + V_H + V_{xc})\psi_{ik} = \varepsilon_{ik}^{DFT}\psi_{ik}$, where ε_{ik}^{DFT} are DFT-like energies, computed on LDA+DMFT charge. We then evaluate

$$E_1 = \text{Tr}(\varepsilon^{DFT}G) \quad (2)$$

and

$$E_2 = -\text{Tr}((V_H + V_{xc})\rho) + E^H[\rho] + E^{xc}[\rho] + E_{nuc-nuc}. \quad (3)$$

Both E_1 and E_2 are computed using Green's function G and density ρ of the solid in the same way as the standard DFT total energy is implemented [11].

The last two terms of Eq. 1 can be computed either from the local Green's function $\hat{P}G$ or from the impurity Green's function G_{imp} . Once the self-consistency is reached, the two are of course equal. We choose to evaluate the second term on the impurity G_{imp}

$$E_3 = \frac{1}{2}\text{Tr}(\Sigma_{imp}G_{imp}) - \Phi^{DC}[\rho_{imp}] \quad (4)$$

However, we never actually use Migdal-Galitskii formula, because it is numerically much less stable than computing the potential energy from the impurity probabilities, i.e.,

$$\frac{1}{2}\text{Tr}(\Sigma_{imp}G_{imp}) = \sum_m P_m E_m^{atom} - \text{Tr}(\varepsilon_{imp}n_{imp})$$

The free energy functional $\Gamma[G]$ (Eq. 2 of the main text) is

$$\Gamma[G] = \text{Tr} \log G - \text{Tr} \log((G_0^{-1} - G^{-1})G) + E^H[\rho] + E^{xc}[\rho] + \Phi^{DMFT}[G_{loc}] - \Phi^{DC}[\rho_{loc}] + E_{nuc-nuc}. \quad (5)$$

First, we extremize it ($\delta\Gamma[G]/\delta G = 0$) to obtain the Dyson equation

$$G^{-1} - G_0^{-1} + V_H + V_{xc} + \Sigma_{DMFT} - V_{dc} = 0. \quad (6)$$

A note is in order here. We assumed $\delta P/\delta G = 0$, which holds whenever the projector does not depend on the self-consistent charge density. To ensure this property, we used for the localized orbitals $|\phi\rangle = \frac{u_l(r)}{r} Y_{lm}(\hat{r})$, where the radial wave function $u_l(r)$ is the solution of the scalar relativistic Dirac equation on the LDA charge density (rather than self-consistent charge density). Note also that the use of the self-consistently determined Wannier functions (which depend on self-consistent charge), as is commonly used in most of the LDA+DMFT implementations [12–14], leads to non-stationary LDA+DMFT solution, and non-stationary free energies.

We next insert the expression $G^{-1} - G_0^{-1}$ into Eq. 5 to obtain expression for free energy

$$\begin{aligned} F = & E_{nuc-nuc} - \text{Tr}((V_H + V_{xc})\rho) + E^H[\rho] + E^{xc}[\rho] \\ & + \text{Tr} \log G - \text{Tr}(\Sigma_{DMFT}G) + \Phi^{DMFT}[G_{loc}] \\ & + \text{Tr}(V_{dc}\rho_{loc}) - \Phi^{DC}[\rho_{loc}] + \mu N \end{aligned} \quad (7)$$

The impurity free energy F_{imp} contains $\Phi^{DMFT}[G_{imp}]$ in the following way

$$F_{imp} = \text{Tr} \log G_{imp} - \text{Tr}(\Sigma_{imp}G_{imp}) + \Phi^{DMFT}[G_{imp}]. \quad (8)$$

In DMFT, $G_{loc} = G_{imp}$ and $\Sigma_{DMFT} = \Sigma_{imp}$, hence we can write

$$\begin{aligned} F = & E_{nuc-nuc} - \text{Tr}((V_H + V_{xc})\rho) + E^H[\rho] + E^{xc}[\rho] \\ & + \text{Tr} \log(G) - \text{Tr} \log(G_{loc}) + F_{imp} \\ & + \text{Tr}(V_{dc}\rho_{loc}) - \Phi^{DC}[\rho_{loc}] + \mu N. \end{aligned} \quad (9)$$

This equation appears as Eq.4 in the main text.

Next we split free energy of the impurity into the energy and the entropy term

$$F_{imp} = E_{imp} - TS_{imp},$$

where

$$\begin{aligned} E_{imp} = & \text{Tr}((\Delta + \varepsilon_{imp} - \omega_n \frac{d\Delta}{d\omega_n})G_{imp}) \\ & + \frac{1}{2}\text{Tr}(\Sigma_{imp}G_{imp}) \end{aligned} \quad (10)$$

Hence

$$\begin{aligned} F = & \frac{1}{2}\text{Tr}(\Sigma_{imp}G_{imp}) - \Phi^{DC}[\rho_{loc}] - TS_{imp} \\ & + E_{nuc-nuc} - \text{Tr}((V_H + V_{xc})\rho) + E^H[\rho] + E^{xc}[\rho] \\ & + \text{Tr} \log(G) - \text{Tr} \log(G_{loc}) + \text{Tr}(V_{dc}\rho_{loc}) + \mu N \\ & + \text{Tr}((\Delta + \varepsilon_{imp} - \omega_n \frac{d\Delta}{d\omega_n})G_{imp}) \end{aligned} \quad (11)$$

Again using the identity $G_{imp} = G_{loc}$ and $\rho_{imp} = \rho_{loc}$ as well as the definition of E_2 (Eq. 3) and E_3 (Eq. 4) we obtain

$$\begin{aligned} F = & \text{Tr} \log(G) + \mu N + E_2 \\ & + \text{Tr}((\Delta - \omega_n \frac{d\Delta}{d\omega_n} + \varepsilon_{imp} + V_{dc})G_{loc}) \\ & - \text{Tr} \log(G_{loc}) + E_3 - TS_{imp} \end{aligned} \quad (12)$$

This equation is implemented in our DFT+DMFT code. Similarly than in the implementation of the total energy Eq. 1, we compute E_3 and TS_{imp} using impurity quantities, while the rest of the terms are computed using the Green's function of the solid. In this way we ensure that F and E are split in the same way between the

”impurity” and the ”lattice” quantities, hence they share almost identical Monte Carlo noise. However, when comparing $E(V)$ and $F(V)$ at two different volumes, $F(V)$ converges faster than $E(V)$ with the number of LDA and/or DMFT iterations.

However, a faster and more stable convergence with MC steps is many times reached by evaluating free energy in a slightly different way. Again using the fact that $G_{imp} = G_{loc}$ and $\rho_{imp} = \rho_{loc}$ we can rewrite

$$F = \text{Tr} \log G + \mu N + E_2 - \text{Tr}(\Sigma_{DMFT} G) \quad (13)$$

$$- \text{Tr} \log G_{imp} + \text{Tr}(\Sigma_{imp} G_{imp}) + E_{imp} \quad (14)$$

$$+ \text{Tr}(V_{dc} \rho_{imp}) - \Phi^{DC}[\rho_{imp}] - TS_{imp} \quad (15)$$

We evaluate Eq. 13 using G of the solid, and Eqs. 14, 15 using impurity quantities.

Notice that $F + TS_{imp}$ can be evaluated at each LDA+DMFT iteration, just like the total energy above. To subtract TS_{imp} at low temperatures, we however need a few extra impurity runs. The method of computing TS_{imp} is explained in the main text (Eq.7 of the main text), and requires the impurity energy at a few temperatures. To calculate the latter, we use

$$E_{imp} = \text{Tr}((\Delta + \varepsilon_{imp} - \omega_n \frac{d\Delta}{d\omega_n}) G_{imp}) + E_{imp-pot}, \quad (16)$$

This is Eq. 6 in the main text. We evaluate different terms in this formula by the following tricks: i) $\text{Tr}(\Delta G_{imp})$ is computed from the average perturbation order $\langle k \rangle$ of CTQMC, and takes the form $\text{Tr}(\Delta G_{imp}) = \langle k \rangle / T$, where T is temperature [5], or, at low temperature it is often more accurate to carry out the Matsubara sum $\text{Tr}(\Delta G_{imp}) = \frac{1}{\beta} \sum_{i\omega_n} \Delta(i\omega_n) G_{imp}(i\omega_n)$. To

achieve fast convergence, we subtract $C/((i\omega_n - E_{imp} - \Sigma_\infty)(i\omega_n - \varepsilon_0))$ and add analytic result for this sum, namely, $C(f(E_{imp} + \Sigma_\infty) - f(\varepsilon_0))/(E_{imp} + \Sigma_\infty - \varepsilon_0)$. Here $C/(i\omega_n - \varepsilon_0)$ is determined to match the high-frequency of $\Delta(i\omega_n)$. ; ii) $E_{imp-pot}$, which is equal $E_{imp-pot} = \frac{1}{2} \text{Tr}(\Sigma G_{imp})$, is computed from the energies of atomic state of QIM E_m^{atom} and their probabilities P_m by $E_{imp-pot} = \sum_m P_m E_m^{atom} - \text{Tr}(\varepsilon_{imp} n_{imp})$ [5], which delivers much more precise interaction energy than obtained by MGF; ii) We spline $\Delta(\omega_n)$ in Matsubara points and determine its derivative $d\Delta/d\omega_n$, and then carry out Matsubara sum by subtracting out the leading high-frequency tails by formula $A/((i\omega - \varepsilon_1)(i\omega - \varepsilon_2))$, which has an analytic sum of $A(f(\varepsilon_1) - f(\varepsilon_2))/(\varepsilon_1 - \varepsilon_2)$. Because the probabilities P_m , hybridization $\Delta(i\omega_n)$ and impurity green’s functions $G(i\omega_n)$ are known to very high precision in CTQMC, the impurity internal energy can easily be computed with precision of a fraction of a meV.

An alternative way to compute the impurity entropy term TS_{imp} is to use the so called ”flat-histogram sampling method” [15], which is also done as postprocessing on self-consistent LDA+DMFT hybridization Δ .

Perhaps, the most challenging term in Eq. 12 to compute is $\text{Tr} \log(G)$, which requires eigenvalues (but not eigenvectors) of the LDA+DMFT eigenvalue problem. We first diagonalize

$$\begin{aligned} (-\nabla^2 + V_{ext} + V_H + V_{xc} + \Sigma(i\omega_n) - V_{dc}) \psi_{i,k,\omega_n} = \\ = \varepsilon_{i,k,\omega_n} \psi_{i,k,\omega_n}. \end{aligned} \quad (17)$$

and then evaluate

$$\text{Tr} \log(G) + \mu N = T \sum_{i\omega_n, i,k,\sigma} (\log(\varepsilon_{i,k,\omega_n} - i\omega_n - \mu) - \log(\varepsilon_{i,k,\infty} - i\omega_n - \mu)) - T \sum_{i,k,\sigma} \log(1 + e^{-\beta(\varepsilon_{i,k,\infty} - \mu)}) + \mu N \quad (18)$$

Here it becomes apparent that if $\Sigma(i\omega_n)$ is frequency independent, the first term in the brackets vanishes, while the second term gives (at $T = 0$) the sum of eigenvalues

$$\text{Tr} \log(G) + \mu N \xrightarrow{U=0} \sum_{i,k,\sigma} \theta(\varepsilon_{i,k} < \mu) \varepsilon_{i,k},$$

the well known DFT contribution to the total energy.

FREE ENERGY FROM THE FUNCTIONAL IN THE HUBBARD MODEL

To demonstrate the efficiency of the proposed method of calculating the free energy within the DMFT method,

we apply it to the single band Hubbard model on the Bethe lattice. In Fig. 1 we show results for the half-filled case in the correlated metallic regime ($U = 2D$), very near the metal-insulator transition.

The upper pannel displays the Free energy calculated from thermodynamics relation (”thermodynamics”)

$$F = E - T(S_\infty - \int_T^\infty \frac{1}{T'} \frac{dE}{dT'} dT') \quad (19)$$

and from the functional, using impurity free energy F_{imp} (”impurity F”), i.e.,

$$F = \text{Tr} \log G - \text{Tr} \log G_{loc} + F_{imp}. \quad (20)$$

The two expressions match within Monte Carlo statistical error. The lower panel shows the entropy computed by both methods. The efficiency of the “impurity F” method is reflected in the fact that for almost all the point in the curve (except the lowest few temperatures $T/D < 0.02$) a single calculation is needed. Namely, to evaluate the integral in Eq. 19 we need to calculate the energy E of the lattice model at all temperatures and then carry out the integral. On the other hand, the formula Eq. 20 does not couple different temperature together, and it requires only the knowledge of the Green’s function and F_{imp} at a single temperature. For $T/D < 0.02$ we were able to calculate F_{imp} from Eq.5 of the main text. For lower temperatures, only a few extra impurity calculations in the temperature range $T < T' < 0.02$ are needed. In Fig. 1 we also display the impurity part of the entropy, defined by $F_{imp} = E_{imp} - TS_{imp}$. It is of course expected that the impurity carries most of the entropy of the system, however, there is also extra contribution due to the coupling of the impurity to the neighboring sites on the lattice, which seems to consistently increase the entropy of the system.

Finally we notice that the same parameter regime was studied in the manuscript by S. L. Skornyakov *et. al.* [16]. Our results disagree with those of Ref. [16], in particular, the entropy at high temperature in the metallic state saturates at $\log(4)$ (not shown in the figure) and not at $\log(2)$ value as in Ref. [16]. This is because at high temperatures all four local states can be accessed leading to 4 degrees of freedom per site. We notice that a shallow plateau appears at $S = \log(2)$, but no saturation.

COMPARISON WITH STANDARD FUNCTIONALS

Here we compare total energy of LDA, PBE [17], and PBEsol [18] functionals with the free energy of LDA+DMFT.

In most weakly correlated solids, LDA underestimates lattice constants on average for 1.6%, while PBE [17] overestimates them for approximately 1%. [19] PBEsol [18] was designed to predict most accurate volumes in solids, and it typically falls in-between LDA and PBE.

In Fig. 2 we compare LDA+DMFT free energy in SrVO_3 with the total energy computed by other functionals. Both LDA+DMFT and PBEsol underestimate lattice constant for approximately 0.6%, while LDA underestimates it for 1.5%, and PBE overestimates for 0.7%. Hence predictions of standard functionals in the case of SrVO_3 are quite in line with standard performance in weakly correlated solids. Perhaps, this is not very surprising given that SrVO_3 is a metallic moderately correlated system.

In FeO (Fig. 3), all standard functionals severely un-

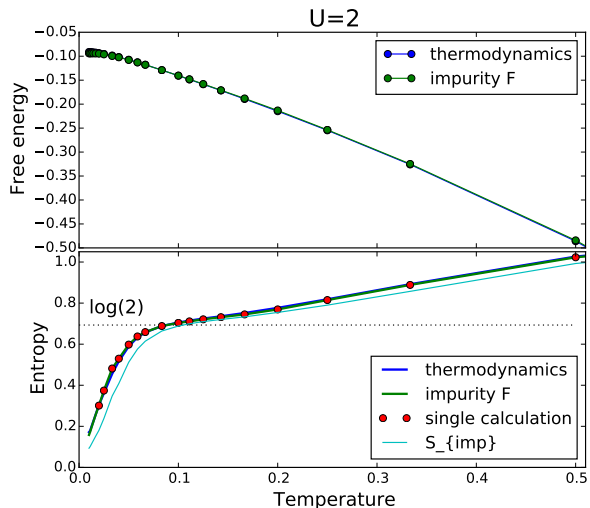


FIG. 1: Free energy and Entropy for the single orbital Hubbard on the Bethe lattice in the correlated metallic regime ($U/D = 2$). Upper panel shows the free energy computed from total energy using standard thermodynamic relations Eq. 19 (“thermodynamics”), and by using impurity free energy in Eq. 20 (“impurity F”). The lower panel shows entropy S computed by the two methods. The same panel also shows the impurity part of the entropy S_{imp} to emphasize that most of the entropy is coming from the impurity part, and very small contribution comes from the DMFT self-consistency condition. The red dots show the points, which were computed by a single DMFT calculation.

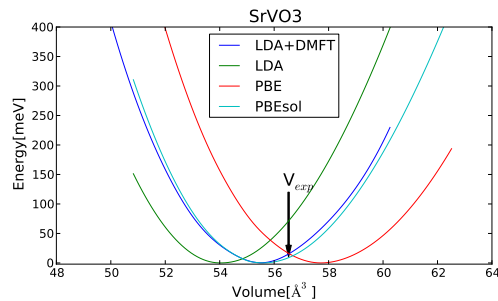


FIG. 2: Free energy of LDA+DMFT for SrVO_3 compared with total energy of other standard DFT functionals.

derestimate volume in the paramagnetic state. For example the lattice constants with LDA, PBEsol and PBE are 7.7%, 6.5% and 5.1% too small, far outside the standard performance of these functionals in weakly correlated solids.

The predictions are improved when the AFM long range order is allowed. LDA and PBEsol still underestimate lattice constant for 3.6%, and 2.3% respectively. On the other hand PBE is this time quite close to the experiment (underestimates for 0.7%). In comparison LDA+DMFT underestimates it for only 0.16%. It is quite clear that the excellent prediction of AFM-PBE

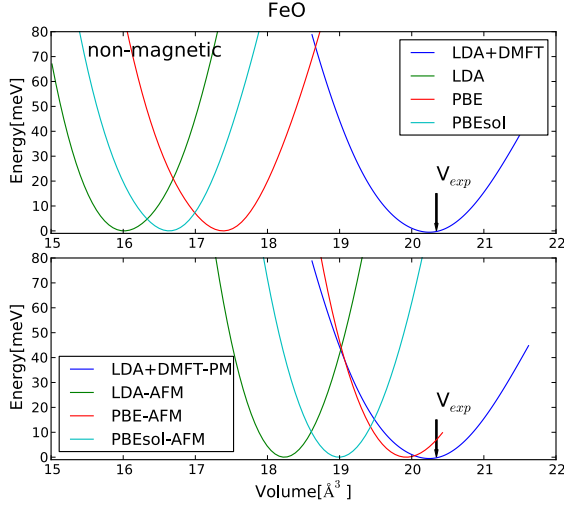


FIG. 3: Free energy of LDA+DMFT for FeO compared with total energy of other standard DFT functionals. Upper (lower) panel shows non-magnetic (antiferromagnetic) DFT calculation. LDA+DMFT results are obtained at 300K in paramagnetic state.

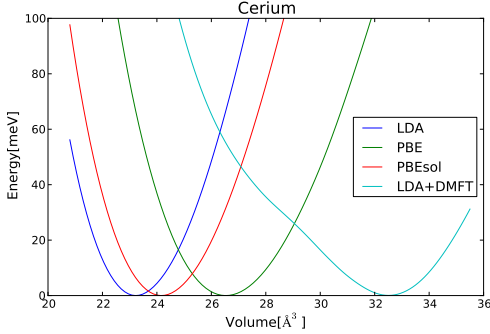


FIG. 4: Free energy of LDA+DMFT for Cerium compared with total energy of other DFT functionals. LDA+DMFT results are obtained at 400 K.

here is merely a coincidence, as normally PBE overestimates the volume.

Finally, we plot results for Cerium in Fig. 4. The result of LDA+DMFT is very different from those of any other functional, as it clearly contains the nontrivial soft mode for the α - γ transition. No other functional shows any hint of such transition.

The equilibrium volume in Cerium is strongly temperature dependent, and is approximately 34\AA^3 at zero pressure and 400 K, while it changes to approximately 28\AA^3 in the α phase at low temperature. The LDA+DMFT results are computed at 400 K, hence at $p = 0$ the volume is somewhat underestimated (1.5%), but under pressure (already at 1 GPa) the agreement with experiment is considerably improved.

The DFT results should be compared to $T = 0$ experimental volume of 28\AA^3 . All functionals underestimate the lattice constant, LDA for 6%, PBEsol for 5% and PBE for 1.8%. Clearly electronic correlations are very important even in the α phase at low temperature, as standard DFT functionals substantially underestimate the volume.

SCREENED COULOMB REPULSION OF YUKAWA FORM

It is noted above that we used the Yukawa representation of the screened Coulomb interaction, in which there is unique relationship between the Hubbard U and Hund's coupling J . If U is specified, J is uniquely determined. To show this we derive the matrix elements of screened Coulomb interaction in our DMFT orbital basis

$$U_{m_1 m_2 m_3 m_4} = \int d^3 r \int d^3 r' \left(\frac{u_l(r)}{r} \right)^2 \left(\frac{u_l(r')}{r'} \right)^2 Y_{l m_1}^*(\hat{\mathbf{r}}) Y_{l m_4}(\hat{\mathbf{r}}) Y_{l m_2}^*(\hat{\mathbf{r}}') Y_{l m_3}(\hat{\mathbf{r}}') \frac{e^{-\lambda|\mathbf{r}-\mathbf{r}'|}}{|\mathbf{r}-\mathbf{r}'|} \quad (21)$$

There exist a well known expansion of Yukawa interaction in terms of spheric harmonics Y_{km} , which reads

$$\frac{e^{-\lambda|\mathbf{r}-\mathbf{r}'|}}{|\mathbf{r}-\mathbf{r}'|} = 4\pi \sum_k \frac{I_{k+1/2}(r_<) K_{k+1/2}(r_>)}{\sqrt{r_< r_>}} \sum_m Y_{km}^*(\hat{\mathbf{r}}) Y_{km}(\hat{\mathbf{r}}') \quad (22)$$

Here $r_< = \min(r, r')$, $r_> = \max(r, r')$, I and K are modified Bessel function of the first and second kind. Inserting this expression into Eq. 21, we get

$$U_{m_1 m_2 m_3 m_4} = \sum_k \frac{4\pi}{2k+1} \langle Y_{l m_1} | Y_{k m_1 - m_4} | Y_{l m_4} \rangle \langle Y_{l m_2} | Y_{k m_3 - m_2} | Y_{l m_3} \rangle \times (2k+1) \int_0^\infty dr \int_0^\infty dr' u_l^2(r) u_l^2(r') \frac{I_{k+1/2}(\lambda r_<) K_{k+1/2}(\lambda r_>)}{\sqrt{r_< r_>}}. \quad (23)$$

Hence, the screened Coulomb interaction has the Slater form with the Slater integrals being

$$F^k = (2k + 1) \int_0^\infty dr \int_0^\infty dr' u_l^2(r) u_l^2(r') \frac{I_{k+1/2}(\lambda r_<) K_{k+1/2}(\lambda r_>)}{\sqrt{r_< r_>}}. \quad (24)$$

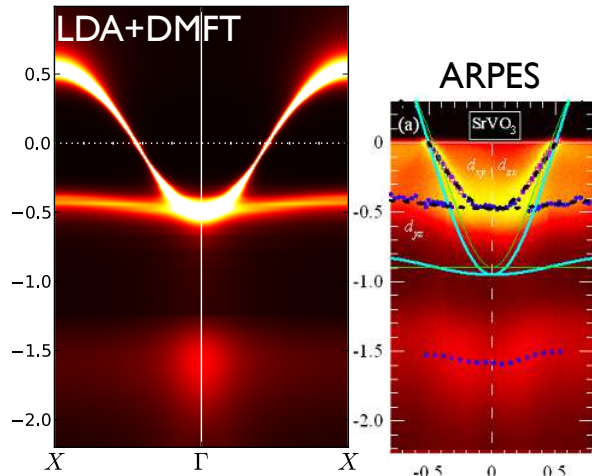


FIG. 5: Spectral function of SrVO₃ within LDA+DMFT at equilibrium volume compared with ARPES spectra of Ref. 20.

This is a product of two one-dimensional integrals and is very easy to efficiently implement.

It is clear from Eq. 24 that λ uniquely determines all F^k 's, and furthermore even one Slater integral (F^0) uniquely determines λ . This is because F^k are monotonic functions of λ and take the value of bare F^k at $\lambda = 0$ and vanish at large λ . Hence given F^0 , the screening length λ is uniquely determined, and hence other higher order F^k are uniquely determined as well.

MASS RENORMALIZATION OF METALLIC SrVO₃

Even though the Coulomb interaction in SrVO₃ is $U = 10$ eV, it gives a relatively moderate mass enhancement over DFT band structure in all-electron LDA+DMFT implementation. This is because the interaction is severely screened by hybridization of d states with oxygen p states, and because the t_{2g} orbitals are in mixed-valence state ($n_{t_{2g}} \approx 1.5$) [3, 4]. In Fig. 5 we show the LDA+DMFT spectral function as well as recent ARPES measurements [20]. The mass renormalization in the t_{2g} orbital is $m_{t_{2g}}^*/m_{band} \approx 2$ and in e_g is $m_{t_{2g}}^*/m_{band} \approx 1.3$. The agreement between ARPES spectra (the experimental signal is color coded on the right) and LDA+DMFT spectral function $A(k, \omega)$ (plotted on the left) is very good, both in the quasiparticle band (between -0.5 eV and 0.5 eV) and Hubbard satellite at -1.5 eV.

-
- [1] K. Haule, C.-H. Yee, and K. Kim, Phys. Rev. B **81**, 195107 (2010), URL <http://link.aps.org/doi/10.1103/PhysRevB.81.195107>.
 - [2] P. Blaha, K. Schwarz, G. K. H. Madsen, D. Kvasnicka, and J. Luitz, *WIEN2K, An Augmented Plane Wave + Local Orbitals Program for Calculating Crystal Properties* (Karlheinz Schwarz, Techn. Universität Wien, Austria, 2001).
 - [3] K. Haule, T. Birol, and G. Kotliar, Phys. Rev. B **90**, 075136 (2014), URL <http://link.aps.org/doi/10.1103/PhysRevB.90.075136>.
 - [4] K. Haule, eprint arXiv:1501.03438v1 (2015), URL <http://arxiv.org/abs/1501.03438>.
 - [5] K. Haule, Phys. Rev. B **75**, 155113 (2007), URL <http://link.aps.org/doi/10.1103/PhysRevB.75.155113>.
 - [6] P. Werner, A. Comanac, L. de' Medici, M. Troyer, and A. J. Millis, Phys. Rev. Lett. **97**, 076405 (2006), URL <http://link.aps.org/doi/10.1103/PhysRevLett.97.076405>.
 - [7] K. Ohta, R. E. Cohen, K. Hirose, K. Haule, K. Shimizu, and Y. Ohishi, Phys. Rev. Lett. **108**, 026403 (2012), URL <http://link.aps.org/doi/10.1103/PhysRevLett.108.026403>.
 - [8] A. McMahan, C. Huscroft, R. Scalettar, and E. Pollock, Journal of Computer-Aided Materials Design **5**, 131 (1998), ISSN 0928-1045, URL <http://dx.doi.org/10.1023/A%3A1008698422183>.
 - [9] B. Amadon, S. Biermann, A. Georges, and F. Aryasetiawan, Phys. Rev. Lett. **96**, 066402 (2006), URL <http://link.aps.org/doi/10.1103/PhysRevLett.96.066402>.
 - [10] J. Bieder and B. Amadon, Phys. Rev. B **89**, 195132 (2014), URL <http://link.aps.org/doi/10.1103/PhysRevB.89.195132>.
 - [11] M. Weinert, E. Wimmer, and A. J. Freeman, Phys. Rev. B **26**, 4571 (1982), URL <http://link.aps.org/doi/10.1103/PhysRevB.26.4571>.
 - [12] H. Park, A. J. Millis, and C. A. Marianetti, Phys. Rev. B **89**, 245133 (2014), URL <http://link.aps.org/doi/10.1103/PhysRevB.89.245133>.
 - [13] H. Park, A. J. Millis, and C. A. Marianetti, Phys. Rev. B **90**, 235103 (2014), URL <http://link.aps.org/doi/10.1103/PhysRevB.90.235103>.
 - [14] D. Grieger, C. Piefke, O. E. Peil, and F. Lechermann, Phys. Rev. B **86**, 155121 (2012), URL <http://link.aps.org/doi/10.1103/PhysRevB.86.155121>.
 - [15] E. Gull, A. J. Millis, A. I. Lichtenstein, A. N. Rubtsov, M. Troyer, and P. Werner, Rev. Mod. Phys. **83**, 349 (2011), URL <http://link.aps.org/doi/10.1103/RevModPhys.83.349>.
 - [16] S. Skornyakov, A. Poteryaev, and V. Anisimov, Physics of the Solid State **57**, 1431 (2015), ISSN 1063-7834, URL <http://dx.doi.org/10.1134/S1063783415070288>.
 - [17] J. P. Perdew, K. Burke, and M. Ernzerhof, Phys. Rev.

- Lett. **77**, 3865 (1996).
- [18] J. P. Perdew, A. Ruzsinszky, G. I. Csonka, O. A. Vydrov, G. E. Scuseria, L. A. Constantin, X. Zhou, and K. Burke, Phys. Rev. Lett. **100**, 136406 (2008), URL <http://link.aps.org/doi/10.1103/PhysRevLett.100.136406>.
- [19] A. E. Mattsson, R. Armiento, J. Paier, G. Kresse, J. M. Wills, and T. R. Mattsson, The Journal of Chemical Physics **128**, 084714 (2008), URL <http://scitation.aip.org/content/aip/journal/jcp/128/8/10.1063/1.2835596>.
- [20] M. Takizawa, M. Minohara, H. Kumigashira, D. Toyota, M. Oshima, H. Wadati, T. Yoshida, A. Fujimori, M. Lippmaa, M. Kawasaki, et al., Phys. Rev. B **80**, 235104 (2009), URL <http://link.aps.org/doi/10.1103/PhysRevB.80.235104>.